Multistep Aggregation Pathway of Human Interleukin-1 Receptor Antagonist: Kinetic, Structural, and Morphological Characterization

Sampathkumar Krishnan and Andrei A. Raibekas*
Department of Pharmaceutics, Amgen, Thousand Oaks, California 91320

ABSTRACT The complex, multistep aggregation kinetic and structural behavior of human recombinant interleukin-1 receptor antagonist (IL-1ra) was revealed and characterized by spectral probes and techniques. At a certain range of protein concentration (12–27 mg/mL) and temperature (44–48°C), two sequential aggregation kinetic transitions emerge, where the second transition is preceded by a lag phase and is associated with the main portion of the aggregated protein. Each kinetic transition is linked to a different type of aggregate population, referred to as type I and type II. The aggregate populations, isolated at a series of time points and analyzed by Fourier-transform infrared spectroscopy, show consecutive protein structural changes, from intramolecular (type I) to intermolecular (type II) β-sheet formation. The early type I protein spectral change resembles that seen for IL-1ra in the crystalline state. Moreover, Fourier-transform infrared data demonstrate that type I protein assembly alone can undergo a structural rearrangement and, consequently, convert to the type II aggregate. The aggregated protein structural changes are accompanied by the aggregate morphological changes, leading to a well-defined population of interacting spheres, as detected by scanning electron microscopy. A nucleation-driven IL-1ra aggregation pathway is proposed, and assumes two major activation energy barriers, where the second barrier is associated with the type I → type II aggregate structural rearrangement that, in turn, serves as a pseudonucleus triggering the second kinetic event.

INTRODUCTION

Aggregation is a dominant degradation pathway of proteins, and can occur during all stages of protein therapeutics processing and storage (1–4). The aggregation of proteins and their deposition into amorphous precipitates or insoluble fibrils were also linked to a number of amyloid diseases, including Alzheimer's and Parkinson's disorders (5–7). The aggregation phenomenon can be caused by protein structural changes or by colloidal effects affecting protein-protein interactions (8–10). Such events can occur via a simple diffusion-limited mechanism (11,12), or may involve nucleation as the primary stage for the further growth and propagation of aggregates (13–15). In previous studies, it became evident that proteins with a dominating β-sheet content are prone to aggregation (16,17), and can self-assemble into either amorphous precipitates or well-defined fibrils (18–20). The aggregation process is also sensitive to a wide range of factors such as protein concentration, hydrophobicity, and charge, as well as solution pH, ionic strength, and temperature (21–25). Despite the critical importance of protein-aggregation problems, the mechanistic details of the aggregation process, including the relationship between kinetic, structural, and gross morphological changes, are poorly understood. Characterizing the different types of aggregates and mechanisms of aggregation could help in combating the aggregates that may pose problems in terms of safety, efficacy, and immunogenicity in vivo, as well as in developing better therapeutic protein formulation strategies.

The use of bioanalytic tools to study the kinetic and structural mechanisms of protein aggregation has evolved over the years (26–28). Size-exclusion chromatography is typically used to quantify the amount of protein-aggregated species and to identify the various soluble forms (dimer, tetramer, or higher species) of aggregates. Other analytical tools, such as dynamic light scattering, analytical ultracentrifugation, field-flow fractionation, and mass spectrometry, can also provide insights into the nature and sizes of soluble aggregates. However, most of these techniques are difficult to apply when it comes to a kinetic growth characterization of significantly larger, insoluble aggregates, and when the aggregation process goes to completion within a short (10–100 min) time.

Highly concentrated human interleukin-1 receptor antagonist (IL-1ra) has the property of aggregating at elevated temperatures, and it can be used as a suitable model for studying aggregation mechanisms of small β-sheet proteins that can occur without protein global unfolding (25,29). It is a 17-kDa member of the IL-1/fibroblast growth factor family of proteins, and is a natural IL-1 blocker that plays an important regulatory role in the inflammation and functioning of the adaptive immune system (30). The protein tertiary structure exhibits a β-trefoil topology (31) and consists of 12 antiparallel β-strands, six of which are arranged in the form of a β-barrel (32,33). In this study, we demonstrate the use of a previously established light-scattering technique (25,34–36) to identify distinct IL-1ra aggregate populations and to analyze their kinetic growth behavior. Then, with additional optical methods, we obtain the structural and morphological

Submitted April 2, 2008, and accepted for publication October 2, 2008.

*Correspondence: andreir@amgen.com

Editor: Feng Gai.

0006-3495/09/01/0199/10 $2.00

doi: 10.1016/j.bpj.2008.10.002

characteristics of isolated time-dependent aggregate species. It was found that the aggregation behavior of IL-1ra emerges as a series of sequential kinetic and structural events that, taken together, suggest a multistep aggregation pathway for this protein at elevated temperatures.

MATERIALS AND METHODS

Purified recombinant human IL-1ra in 10 mM sodium citrate, 140 mM NaCl, and 0.5 mM EDTA, pH 6.5 (CSE buffer), was supplied by an Amgen manufacturing facility as a 220-mg/mL solution. Thioflavin T and 4,4′-dianilino-1,1′–binaphthyl-5,5′-disulphonic acid dipotassium salt (bis-ANS) were from Sigma-Aldrich (St. Louis, MO). All other chemicals were of the highest grade available.

Aggregation assay

The IL-1ra aggregation assay at a constant, elevated temperature (isothermal conditions) was performed in a manner similar to that previously described (25). Typically, 10 mL of IL-1ra stock solution (220 mg/mL protein in CSE buffer) were diluted with the same buffer to corresponding concentrations, and filtered through a 0.2-μm filter (μStar LB, Corning, NY). Unless otherwise specified, the aggregation of IL-1ra was measured using a 96-well glass-bottom plate (Sensoplate, Grenier Bio-One, Frickenhausen, Germany) and a temperature-controlled multidetection plate reader (SpectraMax M5, Molecular Devices, Sunnyvale, CA). According to manufacturer's specifications, the SpectraMax M5 provides a photometric range up to four optical units because of the decreased path length and designed optics. The reported accuracy/linearity for a 0–2 optical unit range is $\pm 1\%$. The sample volume per well was 190 μL. The plates were covered with lids and incubated in the spectrophotometer at 44–48°C, whereas optical density (OD) was measured at 450 nm with 1-min intervals and a 3-s automated shaking step between readings. The shaking step evenly distributes aggregates in the sample well solution before absorbance reading, and minimizes signal errors, particularly during the second kinetic transition. Control (no shaking) experiments showed that the shaking step did not interfere with the protein aggregation propensity in our experimental conditions. The protein concentration was estimated using its absorbance at 279 nm and an extinction coefficient of 13,392 M^{-1} cm^{-1} (25). Absorbance readings at 279 nm were corrected by subtracting the background signal at 650 nm.

Time-dependent aggregates were isolated as follows. The IL-1ra at a concentration of 22 mg/mL in CSE buffer was subjected to an aggregation assay at 47°C. The sample volume per assay well was 200 μL. At a specified time (1000–5200 s), the assay was stopped and the plate was immediately placed on ice. After a 20-min incubation on ice, the aggregation sample was centrifuged (13,000 $\times$ g, 15 min, 10°C), the supernatant was carefully transferred into a new 1.5-mL centrifuge tube, and if necessary, the supernatant volume was adjusted with CSE buffer back to the original 200-μL volume. The aggregated protein fraction (expressed as a percentage) was determined using the difference in absorbance (A_{280}) value between the sample that was not subjected to the aggregation assay (control) and the time point-derived supernatant. For Fourier-transform infrared spectroscopy (FTIR) and scanning electron microscopy (SEM) analyses, aggregate pellets were washed with 10 $\times$ volume of CSE buffer, centrifuged (13, 000 $\times$ g, 15 min, 10°C), and resuspended with 1 $\times$ volume of distilled water.

Analysis of aggregate-type populations

Aggregates of IL-1ra were generated at 47°C, using the plate-reading assay described above. The sample was 22 mg/mL IL-1ra in CSE buffer, and the volume per well was 190 μL. Type I aggregates were generated as the assay run was stopped at the 2500-sec time point, and the sample plate was immediately placed on ice, whereas type II aggregates were generated using a 6000-s incubation. Aggregate sample suspensions were centrifuged down (6000 $\times$ g, 5 min, 12°C), resulting in two separate pellets (type I and type II). Each pellet was resuspended in 200 μL of cold CSE buffer and transferred into a preweighed Spin-X 0.22-μm centrifuge tube filter (Costar, Corning, NY). After centrifugation (6000 $\times$ g, 3 min, 12°C), the filter unit containing dry, aggregated material was weighed again, and the aggregate net weight was calculated. Next, based on the weight estimates, a 10-mg/mL stock aggregate suspension in CSE for each type I and type II was made and subsequently used to prepare 1, 2, 4, 6, and 8 mg/mL samples by dilution with CSE buffer. The OD of sample suspensions was measured at 450 nm, using a SpectraMax M5 plate reader and a 96-well Sensoplate glass-bottom plate. The sample volume per well was 200 μL.

Treatment of isolated type I aggregates at 47°C

Type I aggregates were generated using 96-well plates and the same conditions as described above, using 22 mg/mL IL-1ra solution in CSE (190 μL per well, 12 samples) at 47°C. After a 2500-s incubation (near the end of the first aggregation phase), the experiment was stopped and the plate was immediately transferred onto ice. After a 20-min incubation on ice, samples were pooled and centrifuged (13,000 $\times$ g, 7 min, 10°C), and the supernatant was discarded. The pellet was washed with 400 μL cold CSE buffer, centrifuged as described above, and resuspended in 100 μL of cold CSE buffer. A 50-μL aliquot of type I aggregate suspension from the previous step was subjected to a 40-min incubation at 47°C, using a programmed thermal incubator (Mastercycler, Eppendorf, Hamburg, Germany). The sample was then cooled down to 4°C and used for FTIR analysis. The other untreated 50-μL portion of the sample (stored at 4°C) was used as a control.

Dye-tracer assay

This assay was performed using a 96-well glass-bottom plate (Sensoplate) and a temperature-controlled plate reader, SpectraMax M5 (fluorescence mode). The sample volume per well was 193 μL. The plate was covered with a lid and was incubated in the spectrophotometer at 47°C, while the fluorescence emission was monitored at 500 nm (excitation at 420 nm), with 1-min intervals and a 3-s automated shaking step between readings. The bottom-well reading mode was used for fluorescence measurements.

The sample solution (per well) was prepared by mixing 190 μL of 22 mg/mL IL-1ra solution in CSE buffer with either 3 μL of 10 mM thioflavin T or 3 μL of a 0.3 mM bis-ANS stock solution in CSE, to achieve dye/protein molar ratios of 0.125 and 0.0037, respectively. These ratios were chosen on the basis of a prescreening study, as described below. First, a set of sample solutions containing a wide range of dye/protein ratios plus a control (no dye) was subjected to a standard aggregation assay measuring the OD_{450} signal. Then a fresh set of samples, with ratios that did not show OD aggregation kinetic deviations from the control, were subjected to a fluorescence-based aggregation assay (see above). Based on these data, two dye/protein ratio sets (0.125 and 0.0037) that displayed a mutually comparable fluorescence intensity range during the assay, and therefore could be run in a single experiment, were chosen for the main study. In a separate experiment, dye selectivity was assessed using the above ratios for thioflavin T and bis-ANS. The sample solutions (in triplicates) were prepared as above, the aggregation assay was performed for 110 min (6600 s), and the aggregates were separated from the soluble protein fraction by centrifugation (13,000 $\times$ g, 10 min, room temperature). The measured volume of the supernatant (soluble fraction) was 160 μL, so the aggregate fraction was also resuspended in 160-μL CSE buffer, and then the dye-related fluorescence intensity (excitation at 420 nm; emission at 500 nm) of each soluble and resuspended aggregate fraction was measured and compared, using the Sensoplate and SpectraMax M5 instrument. We determined that the vast majority of fluorescence signal (95% and 99.9% for thioflavin T and bis-ANS, respectively) was associated with the suspended aggregate fraction. In addition, the selective binding of thioflavin T to the aggregate fraction was independently confirmed with fluorescence-based microscopy, using a BX51 system microscope equipped with a fluorescence illuminator (Olympus Corp., Melville, NY).

Crystalline precipitation of IL-1ra

A 2-mL solution of 220 mg/mL IL-1ra in CSE buffer was dialyzed against 3.5 L of water at 4°C, using a Slide-A-Lyzer 10 K dialysis unit (Pierce, Rockford, IL). After 3 days of dialysis, the sample became partially precipitated or cloudy. Next, the sample was removed from the dialysis unit, immediately placed on ice, and after a 20-min incubation on ice, was centrifuged (3000 × *g*, 5 min, 6°C). The supernatant was discarded, and the pellet was resuspended in 4 mL of ice-cold water and centrifuged under the above conditions (wash step). The wash step was applied one more time, the supernatant (water) was discarded, and the pellet was placed in 100-μL ice-cold water and stored at 4°C until further use. The crystalline nature of the precipitate was confirmed by both SEM and transmission electron microscopy.

Fourier-transform infrared (FTIR) spectroscopy

The FTIR spectra of the native and aggregated protein fractions in CSE buffer were acquired using a Bomem Prota infrared spectrometer (ABB USA, Norwalk, CT). Samples were placed in a BioTools (Jupiter, FL) liquid sampling cell, equipped with CaF_2 windows that provided a 6-μm path length. For each spectrum, a 128-scan interferogram was collected in single-beam mode, with a 4-cm^{-1} resolution. All second-derivative spectra were baseline-corrected using the instrument software, based on the method of Dong and Caughey (37), and were area-normalized under the second-derivative amide I region, at 1600–1700 cm^{-1} (38).

Scanning electron microscopy (SEM)

A sample volume of 10 μL for each preparation was deposited onto SEM stubs covered with double-sided adhesive tape. The droplet was spread across the surface of the tape, using the pipette tip, and was allowed to air-dry. The stubs were then placed into the vacuum chamber of a Pelco SC-7 sputter-coating device (Ted Pella, Redding, CA), and the chamber was evacuated. The samples were conductance-coated with gold-palladium under standard conditions, and were examined using a scanning electron microscope (model ESEM XL30, FEI Co., Hillsboro, OR) at 5 or 10 kV. Control experiments with the native protein alone did not reveal any aggregates.

Aggregation rate analysis

The observed rate of aggregate formation (ν) was determined by the linear extrapolation of the time-dependent OD_{450} change within the growth region. The rate ν was obtained from the slope of the plot of steepest part of the OD_{450} value change for each aggregation transition versus time (units per hour) (39). Because protein aggregates had a quantitative linear correlation with the OD_{450} change within each transition, but because the relative OD_{450} change for the same amount of aggregates was greater for the first transition by a factor of 5.304 (Fig. 1 *B*), for the transition-based comparative kinetic analysis, we used normalized first-transition rates (i.e., $\nu_{n,1st} = \nu_{1st,obs}/5.304$). The reaction order was determined based on the "method of initial rates" (40), from the slope of the linear fitted ln-ln plot of ν versus protein molar concentration.

RESULTS

IL-1ra aggregation kinetic behavior

A well-defined biphasic aggregation kinetic trace was observed, using a combination of protein concentrations (12–27 mg/mL) and incubation temperatures (44–48°C). This phenomenon is illustrated in Fig. 1 *A*, which shows an aggregation profile of 22 mg/mL IL-1ra at 47°C, as monitored by an OD signal at a 450-nm wavelength (OD_{450}). At

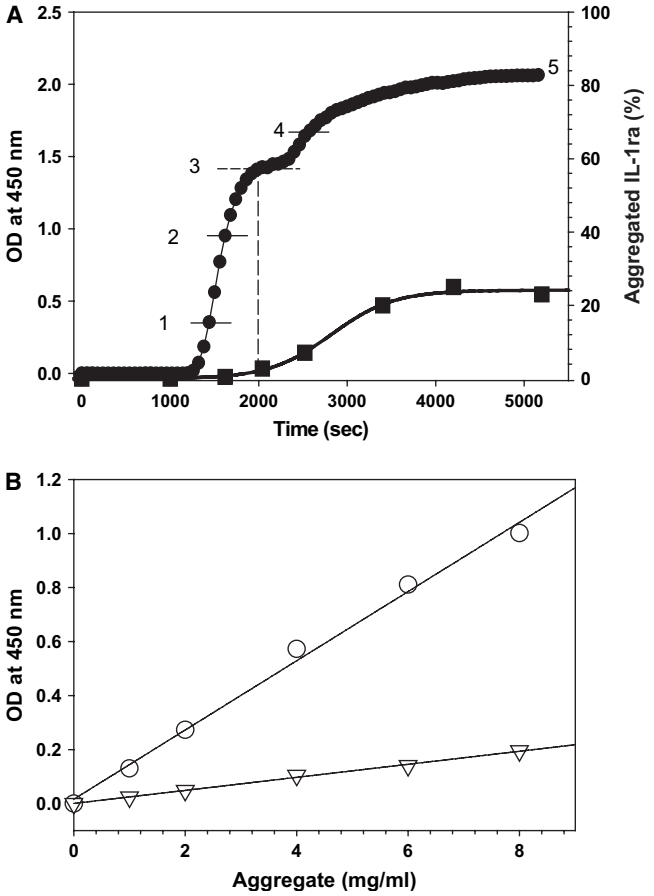

FIGURE 1 Aggregation of 22 mg/mL IL-1ra in CSE buffer, pH 6.5, at 47°C. (*A*) Aggregation kinetic profile (*solid circles*) and corresponding estimates of aggregated protein (*solid squares*), as described in detail in Materials and Methods. Five different time points from which aggregates were collected for further analyses are indicated on kinetic plot. (*B*) Relationship between OD_{450} and amount of suspended aggregate. Plots are shown for isolated aggregate populations associated with first (type I, *open circles*) and second (type II, *open triangles*) kinetic transitions.

this temperature and protein concentration, the protein has a lag phase, followed by a steep growth phase corresponding to the formation of protein aggregates. After reaching a plateau (at ~2000 s), a second lag phase is evident before the onset of the second growth phase that exhibits relatively less OD_{450} change compared with the first transition. This is followed by the termination phase. The remaining soluble protein concentration was determined at various time points by absorbance at 280 nm, and this fraction was subtracted from the total initial protein to estimate the amount of aggregates as percentage of total protein (as detailed in Materials and Methods). The remaining soluble fraction of IL-1ra retained the physical and structural properties of the native protein according to its FTIR spectrum and size-exclusion chromatographic profile (data not shown). Generally, the solution IL-1ra secondary structure was not perturbed at 44–48°C, according to FTIR (data not shown) and CD (circular dichroism) (at up to 55°C) spectral data analyses (25,29).

The results are plotted in Fig. 1 *A* along the right-hand *y* axis, which illustrates that the aggregated protein corresponding to the first transition of the OD_{450} aggregation profile (between 1000–2000 s) constitutes only a small fraction (<5%) of the total protein. On the other hand, the second transition is responsible for the aggregation of an additional 20% of the total protein, although its relative change in OD_{450} signal is ~3 times lower than that observed in the first transition.

This observation led us to hypothesize that each transition represents an accumulation of structurally different aggregate populations (i.e., type I and type II aggregates), where the type II population has the property of scattering less light, resulting in a lower OD signal. Therefore, in the next step, the OD_{450} values of isolated type I and type II aggregate suspensions were compared directly (as detailed in Materials and Methods). As shown in Fig. 1 *B*, the OD change displays a linear dependence on aggregate concentration, regardless of aggregate type. However, the slope of the type II curve is ~5× lower than the slope of the type I curve. This is in agreement with the above kinetic data, supporting the idea of at least two distinctive aggregate population types formed during the IL-1ra aggregation process.

Structural and morphological properties of IL-1ra aggregates

To gain greater insight into protein aggregate populations, we analyzed the washed insoluble aggregates obtained at five consecutive time points (Fig. 1 *A*), using FTIR spectroscopy. As seen in Fig. 2 *A*, the second-derivative FTIR spectrum of the native IL-1ra in solution exhibits a predominantly β-sheet structure, with characteristic minima at 1643 cm^{-1} and 1632 cm^{-1}. Upon aggregation, the first time point, corresponding to the early growth phase of the first transition, shows a shift from 1643 cm^{-1} (intramolecular β-sheet structure) to 1632 cm^{-1}. This is accompanied by a transition from 1689 cm^{-1} to 1692 cm^{-1}, indicating the simultaneous growth of the intermolecular β-sheet structure (8,37). The shift of the main peak toward the lower frequency-absorbing β-sheet structure continues until the end of the first transition. The third time-point aggregates, taken at the end of the first transition, displayed broad bands at 1632 cm^{-1} and 1622 cm^{-1}, suggesting the presence of both native β-sheet and nonnative intermolecular β-sheet structures (Fig. 2 *B*). This shift also indicates a further growth of IL-1ra aggregates, as previously demonstrated (41). When the protein aggregation process enters the second transition (fourth time point), aggregates show a major growth of the nonnative 1624-cm^{-1} band, as well as the 1685-cm^{-1} band. By the end of the second transition (fifth time point), there is a clear shift from the native structure to the nonnative β-sheet structure. In addition, the first-transition FTIR spectra produce a well-defined isosbestic point around 1630 cm^{-1} that is shifted to ~1625 cm^{-1} during the second transition (Fig. 2 *B*). Taken together,

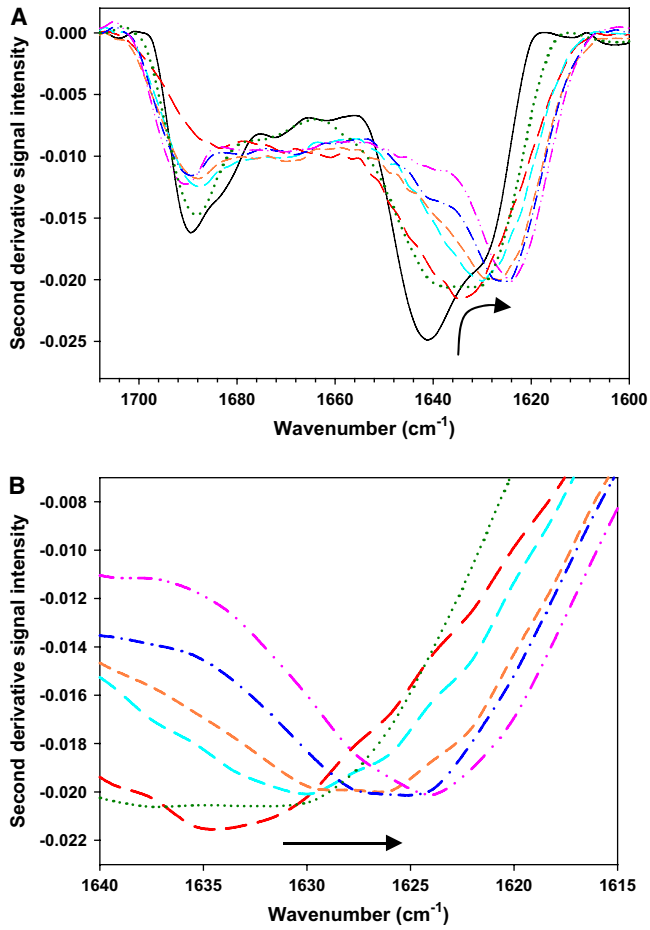

FIGURE 2 Second derivative FTIR spectra show protein structural changes in IL-1ra aggregates isolated at time points indicated in Fig. 1. Direction of spectral change is indicated by arrow. (*A*) Control native protein in solution (*solid black line*), followed by aggregates at first (*long red dashed line*), second (*medium cyan dashed line*), third (*short orange dashed line*), fourth (*blue dotted and dashed line*), and fifth (*pink double dotted and dashed line*) time points. Also shown are FTIR data of protein in crystalline state (*green dotted line*). (*B*) Detailed view of overlaid FTIR spectra demonstrates how type I aggregates (time points 1–3) undergo a consecutive structural transition and display more of the intramolecular β-sheet structure at 1638–1628 cm^{-1}, which is converted into intermolecular β-sheet at 1622 cm^{-1} and 1695 cm^{-1}, as seen in type II aggregates (time points 4–5).

the data suggest two structurally different protein assemblies within the type I (first transition) and type II (second transition) aggregates.

Fig. 2 *A* also shows the FTIR spectrum of the IL-1ra crystalline state obtained, as described in Materials and Methods. The crystalline protein has more of the low-frequency 1632-cm^{-1} band, probably because of closer packing. This spectrum closely resembles the early phase (first time point) of the first aggregation transition, suggesting that the protein conformations in crystals and the early type I aggregates may be similar. One significant difference was that, unlike aggregates, the crystalline state was reversible, and when crystals were dissolved in CSE buffer at room temperature,

they turned into a protein solution that exhibited a native (structurally unperturbed) FTIR spectrum (data not shown).

Because the FTIR data indicated a sequential type I → type II structural transition of aggregates formed during the process, we investigated the structural flexibility of isolated type I aggregates. The spectrum of type I aggregates collected at the end of the first transition of 22 mg/mL protein at 47°C is shown in Fig. 3. Aggregates were centrifuged and washed several times to remove any remaining (unbound) protein in solution (see Materials and Methods), and were then incubated in suspension at 47°C for ~40 min. This treatment resulted in a further structural transition to the nonnative 1622-cm^{-1} and 1692-cm^{-1} intermolecular β-sheet structure, resembling the spectral shift characteristic of type II aggregates (Figs. 2 and 3), and suggesting that at the end of first transition, the protein in type I aggregates can undergo a structural rearrangement. Consequently, this rearrangement could precede and predetermine the second transition, i.e., could serve as a pseudonucleation step for the next, type II aggregation event. The morphological properties of aggregates collected at time points 1–5 were studied using SEM, and the results are shown in Fig. 4. All aggregates were free of soluble protein (washed) before examination by SEM. The aggregates at the first time point are essentially dense clusters of highly fused spherical particles, each of which is ~0.5 μm in diameter. As the aggregation process progresses, the spheres continue to develop, possibly because of the independent growth or the fusion of smaller spheres. By the end of the first transition (third time point), the spheres approach 1–1.5 μm in diameter. The second transition aggregates (time points 4 and 5) show a significant enlargement of individual spheres, and in some cases reach more than 3 μm in diameter. Although individual spherical particles become well-developed and less fused (defused), they all remain interconnected or chained within the aggregate cluster. As shown in Fig. 1, the second transition aggregates recruit the major fraction of the soluble protein, but display a lower relative OD_{450} change. Taken together with the FTIR and SEM analyses, these results suggest a sequential kinetic and structural aggregation process, where the second transition, as triggered by the first transition, independently recruits soluble protein molecules from solution. This would lead to a predominantly individual aggregate development, resulting in chains of partially defused large spherical particles and, as shown in Fig. 1, less packed aggregate clusters.

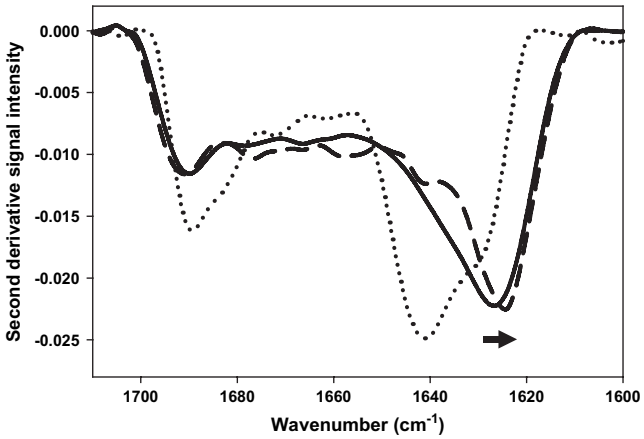

FIGURE 3 IL-1ra second derivative FTIR spectra show protein structural changes within isolated type I aggregates after incubation at 47°C. Overlaid type I protein-aggregate spectra before (*solid line*) and after (*dashed line*) incubation are shown. Reference spectrum of native protein in solution is also indicated (*dotted line*). Aggregated protein alone is capable of type I → type II structural rearrangement, as indicated by arrow.

We evaluated aggregation kinetics further by using the fluorescent dyes bis-ANS and thioflavin T as aggregation kinetic tracers, using similar OD-based assay conditions as above, but monitoring the dye fluorescence intensity instead. In this particular case, the initial purpose was to confirm the biphasic shape of the aggregation kinetic curve, using an alternative, OD-independent mode of detection. The assay was designed such that the fluorescent dye would interact (coaggregate) selectively with the aggregated fraction rather than with the soluble protein fraction, and therefore would function as a tracer for the aggregation process. This was achieved by using a specific dye/protein molar ratio of 0.125 and 0.0037 for thioflavin T and bis-ANS, respectively (as detailed in Materials and Methods), resulting in ~155-μM thioflavin T and 4.7-μM bis-ANS assay sample solutions. We should note that, according to Roy et al. (41), although bis-ANS analog 8-anilinonaphtalene-1-sulfonate (ANS) can interact with IL-1ra, affect its tertiary structure, and even promote IL-1ra aggregation, these effects were achieved using a relatively high (4–21 mM) ANS concentration, and at least equal or five times higher molar amounts of ANS over the protein in the sample solution. Alternately, Latypov et al. (42), using high-resolution NMR, found no evidence for ANS-induced partially denatured or aggregated forms of IL-1ra with lower ($\leq$0.5 mM) ANS concentrations.

The primary choice of tracers was driven by their different modes of interaction with proteins, resulting in increases in tracer fluorescent emission. Although bis-ANS acts as a general hydrophobic surface probe (43), thioflavin T is a specific probe for the pleated β-sheet conformation (44). Fig. 5 shows the OD_{450} aggregation profile of the protein, along with the fluorescent traces of both dyes observed during their coaggregation with IL-1ra at 47°C. There is no detectable increase of fluorescence during the lag phase (0–1100 s), indicating that each dye selectively traces only the aggregation process. The bis-ANS and OD_{450} traces are very similar in showing two kinetic transitions. However, the second transition in the bis-ANS trace dominates, insofar as its fluorescent signal is less likely to be influenced by the type I-type II changes in aggregate cluster packing. Overall, the bis-ANS tracer data correlate with the aggregation assay (OD_{450}) biphasic kinetic data, as well as with the difference in amount of accumulated type I and type II aggregates (Fig. 1 *A*). On the other hand, the change in fluorescence

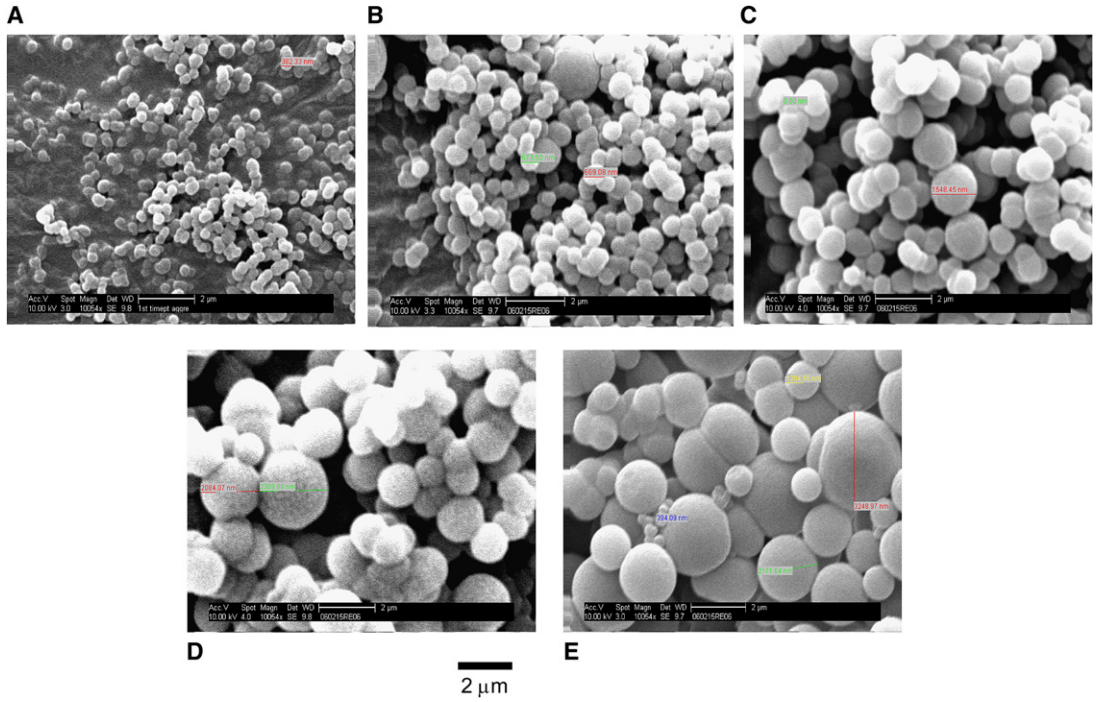

FIGURE 4 Scanning electron micrographs show morphology of IL-1ra aggregates collected at time points 1–5 (*A–E*). Magnification, ×10,000. (*A* and *B*) Time points 1 and 2 represent type I transition, and show average growth of aggregates from 0.5 to 1.0 μm diameter. (*D* and *E*) Time points 4 and 5 represent type II transition, and demonstrate further aggregate growth up to 3.3-μm diameter. (*C*) Time point 3, with 1–1.5-μm diameter aggregates, represents midpoint between transitions. A 2-μm scale bar is shown below *D*. See Results for more details.

upon the coaggregation of thioflavin T shows a unique profile, lacking the type I kinetic transition (Fig. 5). Thioflavin T was shown to bind to nonnative β-sheet intermolecular contacts in aggregates with a corresponding increase in fluorescence (within a 480-nm region), and is used to track the growth of amyloid fibrils (45,46). In the case of IL-1ra, thioflavin T interacts exclusively with type II aggregates, as indicated by the absence of the first transition in the fluorescence kinetic trace. This is in agreement with the FTIR data and confirms that, unlike type I, the type II aggregates are assembled via intermolecular β-sheet interactions. The fluorescent tracer results clearly show the difference in structural nature of type I and type II aggregates, and support the FTIR-observed aggregate structural transitions.

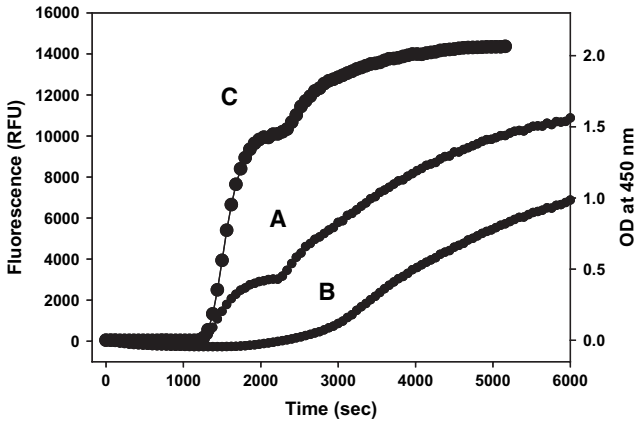

FIGURE 5 Dye-tracer aggregation kinetic profiles of 22 mg/mL IL-1ra in CSE at 47°C, as monitored by bis-ANS (*curve A*) and thioflavin T (*curve B*) fluorescence. Ex = 420 nm, and Em = 500 nm (see Materials and Methods for details). The OD_{450} trace (*curve C*) from Fig. 1 is shown as a reference.

Effect of temperature and protein concentration on IL-1ra aggregation rates

The aggregation kinetics of IL-1ra was dependent on protein concentration and temperature increase. The first (type I) transition lag phase became shorter, suggesting a faster nucleation event (47). This was followed by an overall faster first transition, a shorter first-transition termination phase (equal to the type II lag phase), and finally, a faster second transition (data not shown).

Fig. 6 *A* shows the aggregation-rate analysis of the 27-mg/mL protein assayed at 44–48°C (317–321 K). The kinetic rates (ν) for the aggregation of both transitions were determined as described in Materials and Methods, using the integral method and plotted as a function of temperature (K) (Fig. 6 *A*). Both transitions show a linear dependence of aggregation rates on temperature but are different in their slopes, indicating a higher first-transition rate constant. Fig. 6 *B* illustrates the dependence of aggregation rates on the initial protein concentration at constant temperature, showing that at 47°C, the aggregation rates of both transitions gradually become higher as the concentration increases

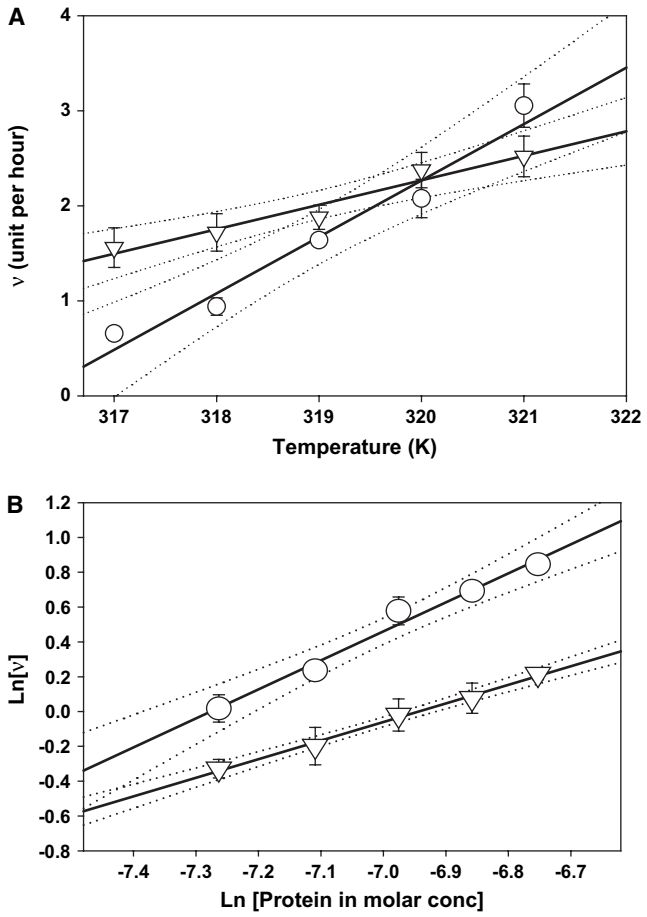

FIGURE 6 Effect of temperature and protein concentration on IL-1ra aggregation rates. IL-1ra is in CSE buffer, pH 6.5. (*A*) Observed aggregation rates (ν, unit/h) for first (*circles*) and second (*triangles*) transitions of aggregation are plotted against temperature (K). Protein concentration is 27 mg/mL. Error bar represents standard deviation of seven samples. (*B*) The ln-ln plot of ν (unit/h) versus protein molar concentration. Temperature is 47°C. First (*circles*) and second (*triangles*) kinetic transition data are plotted and linearly fitted, showing slope values of 1.67 and 1.06, respectively. Error bar represents standard deviation of three samples. Dotted lines represent 95% confidence intervals for slopes. See Materials and Methods for experimental details.

from 12 to 20 mg/mL. The observed aggregation rates within the same aggregate type were plotted against protein concentration (Fig. 6 *B*), and the slope of the linear fitted ln-ln plot was used to obtain the reaction order. It was estimated that under our experimental conditions, the first (type I) transition of aggregation was more of a second-order reaction (slope = 1.67), whereas the second (type II) transition clearly followed a first-order reaction process (slope = 1.06).

DISCUSSION

Previously (25), we investigated the aggregation of highly concentrated (100–140 mg/mL) IL-1ra upon incubation at 39–42°C, and the aggregation kinetic trace displayed a single-transition (sigmoid) profile consisting of a prolonged lag phase, followed by phases of linear growth and plateau. Here, we induced protein aggregation at lower (12–27 mg/mL) protein concentrations and slightly higher (44–48°C) temperatures, without perturbing the protein secondary structure (25,29). These new conditions led to a more complex, biphasic kinetic behavior. In fact, when aggregates resulting from the previously reported (25) single-transition aggregation kinetic process were generated, isolated, and subjected to FTIR and SEM analyses, they displayed properties of type I aggregates (data not shown). This indicates that the type II aggregation transition can be largely suppressed at certain combinations of protein concentration and temperature.

Altogether, the kinetic, structural, and morphological data suggest a multistep mechanism of thermally induced aggregation of IL-1ra, as schematically depicted in Fig. 7. The rationale behind the mechanism steps is as follows. Previous studies indicated that both protein aggregation and crystallization are nucleation-dependent kinetic processes that could be intrinsically linked at an early stage preceding nucleus formation (48,49). This could be the case for IL-1ra, because the secondary structure of the crystal-packed protein is similar to the structure of the protein packed in the early aggregates (Fig. 2, *A* and *B*). The IL-1ra crystal cell unit contains two protein molecules positioned such that they would form an asymmetric dimer, perhaps because of the cation-pi interactions linking them to the earlier, prenucleation stage of the protein crystallization and aggregation kinetic processes (25,33). Therefore, the IL-1ra asymmetric dimer-like assembly stabilized by cation-pi interactions could be the earliest intermolecular precursor of type I aggregation, as indicated by the M* state (Fig. 7).

The aggregated protein undergoes a structural transition, evidenced by loss of the 1942-cm^{-1} high-frequency β-sheet band and the appearance of the 1632-cm^{-1} low-frequency β-sheet band. Most striking is the conversion of the 1689-cm^{-1} β-turn band and the formation of nonnative bands at 1622 cm^{-1} and 1692 cm^{-1} (Fig. 2 *A*). This may be concomitant with the property of the nucleation state shown in Fig. 8 as M_a, facilitating continuous growth of the type I aggregate ($M_a \rightarrow M_b$). The protein forms a clustered population of small spheres that are ~0.2–0.5 μm in diameter (Fig. 4, *A* and *B*) and that has native 1632-cm^{-1} and nonnative 1622-cm^{-1} IR bands (Fig. 2 *A*). The type I aggregate population continues to grow, developing spheres that, by the end of the third time point, reach nearly 1.5 μm (Fig. 4 *C*). The protein assembly in aggregates at this stage is indicated by M_x on the scheme. The secondary structure of the protein starts showing significant changes as the low-frequency β-sheet band at 1632 cm^{-1} begins to shift to the nonnative 1622-cm^{-1} band.

Consequently, the protein in the aggregates overcomes a second energy barrier to form M_x*, resulting in a structural rearrangement because of increased internal energy. This structural transition forms a pseudonucleus with an altered,

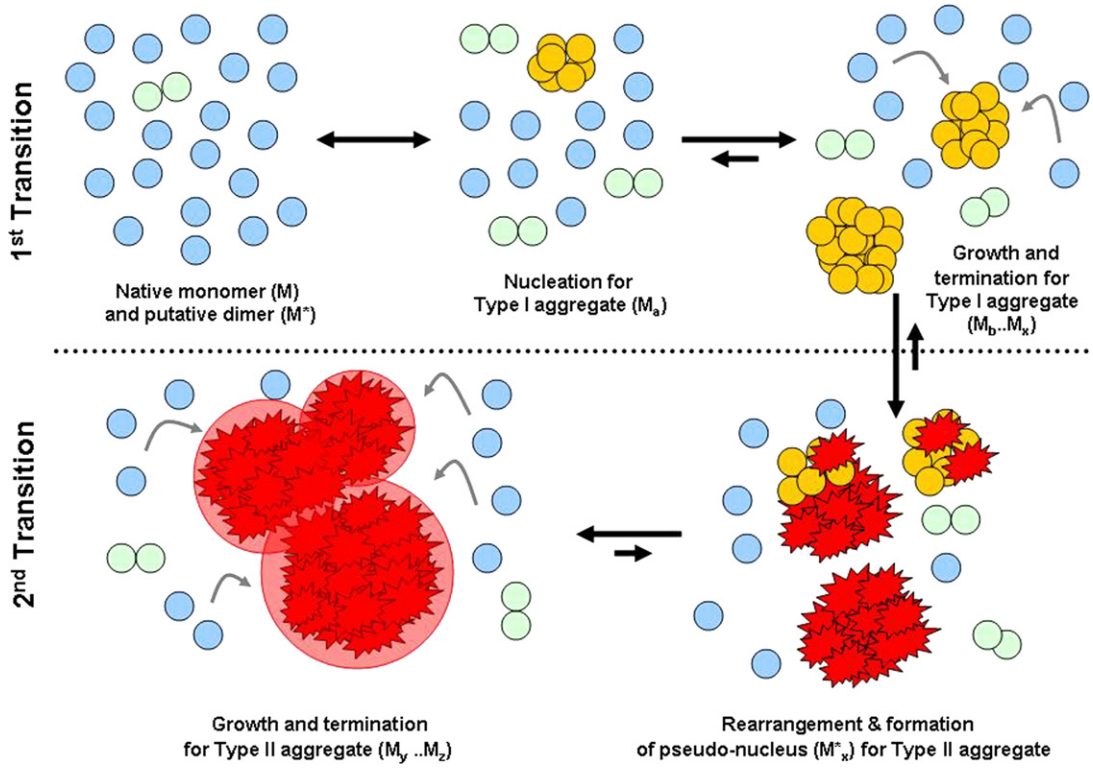

FIGURE 7 Schematic drawing of proposed IL-1ra aggregation pathway at elevated temperatures. Monomer (M) and dimer (M*) are blue single and green double circles, respectively. Both nucleus (M_a) and type I aggregates (M_b … M_x) are clusters of yellow circles. The rearrangement of type I aggregates into a pseudonucleus (M^*_x) is indicated by red asterisk clusters. Type II aggregates (M_y … M_z) are asterisk-filled red circles. See Discussion for more details.

possibly greater hydrophobic surface of aggregates, resulting in favorable nonnative intermolecular contacts that initiate type II aggregation. The type II growth phase may be propagated in this way, resulting in a massive and cooperative recruitment of protein molecules from solution as they are efficiently packed into the aggregate developing spheres (M_y). The protein is tightly packed in the aggregates because of a stronger intermolecular β-sheet signal, as evident in the shift of IR bands to 1622 cm^{-1} and 1694 cm^{-1}. The large 3–4-μm individual aggregates could be further developed by the fusing of smaller aggregate spheres to some extent, as seen in micrographs associated with the fourth and fifth time points (Fig. 4, *D* and *E*) and as indicated by M_z species in the scheme. Unlike the type I aggregation, the type II aggregation appears to be a first-order reaction process (Fig. 6 *B*), suggesting direct protein self-assembly into a spherical body.

The observed conformational flexibility of the type I IL-1ra aggregates (Fig. 3) seems to be in accordance with the aggregation behavior of some other β-sheet proteins. For example, Cerda-Costa et al. (50) reported on the double nature of very early aggregation kinetics of ADA2h, proposing a step model of aggregation in which the denatured polypeptide first folds into an aggregated β-intermediate,

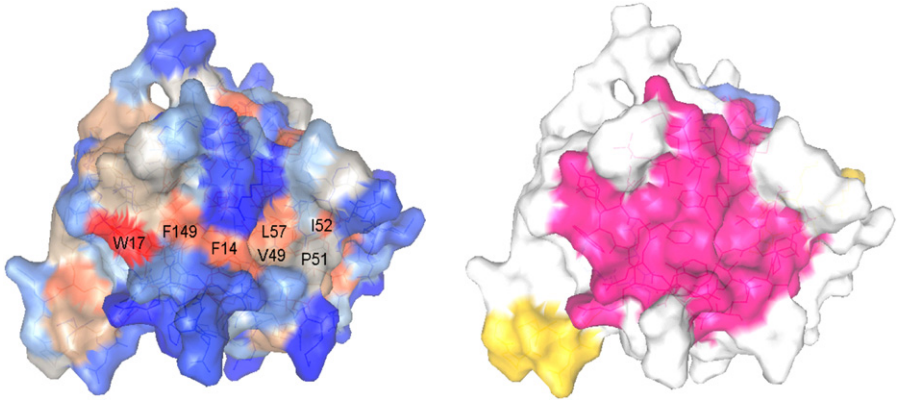

FIGURE 8 Crystal structure-based IL-1ra surface analysis suggests an exposed β-sheet with a hydrophobic channel. The surface distribution was analyzed using a 3D Molecule Viewer (Invitrogen, Carlsbad, CA) and the Protein Data Bank coordinate file 1ILR. The β-sheet is shown in red (*right*). The putative hydrophobic channel is contributed by residues W17, F149, F14, V49, L57, P51, and I52 (*left*). Residue number accounts for the presence of an extra N-terminal methionine in the recombinant protein.

subsequently reorganizes into a more ordered β-sheet structure, and finally results in amyloid fiber formation. Serio et al. (51) reported that the critical region of one prion protein, Sup35, is initially unstructured in solution, and then forms self-seeded amyloid fibers. They examined the in vitro mechanism by which this state is attained and replicated. Structurally fluid oligomeric complexes appear to be crucial intermediates in de novo amyloid nucleus formation. Serio et al. (51) also observed that rapid assembly ensues when these complexes conformationally convert upon association with nuclei.

Both aggregation kinetic transitions (and the first one in particular) are sensitive to even slight increases in temperature (Fig. 6 *A*), supporting the idea of hydrophobic interactions at play. The type I aggregates of IL-1ra observed in our study bound only to bis-ANS, whereas type II aggregates interacted with both bis-ANS and thioflavin T dyes (Fig. 5). This indicates that type I population growth proceeds primarily via hydrophobic interactions, whereas at an earlier, prenucleation stage, electrostatic interactions can also play a significant role (25). Type II aggregates can also be grown by hydrophobic-driven packing, as indicated by increased bis-ANS binding. At the same time, they are clearly distinctive because of the intermolecular β-sheet hydrogen bonding shown by both thioflavin T binding and the strong, nonnative β-sheet bands observed using FTIR. This finding is in agreement with the work of Chiti et al. (52) on the kinetic partitioning of protein folding and aggregation of human acylphosphatase, where a hydrophobic region with β-sheet propensity appeared to be the major factor governing this protein-aggregation process. In the case of IL-1ra, native-like hydrophobic intermolecular interactions are possible as the crystal structure-based surface analysis suggests at least two putative hydrophobic clusters contributed by either W17 or W120 residues. As illustrated in Fig. 8, one of them, a channel-like hydrophobic region, is indeed colocated with the surface-exposed β-sheet.

The described biphasic aggregation kinetics of IL-1ra is the most clearly defined example in protein aggregation. Remarkably, it closely resembles a theoretical model for a biologistic process of growth with sequential taxonomy (53). Yet the question remains: why would IL-1ra aggregation permit such sequential kinetic events? One plausible explanation involves considering IL-1ra solution (any fixed composition, e.g., 22 mg/mL protein in CSE buffer) as a closed thermodynamic system in its metastable equilibrium state that can also permit two subsequent, lower-energy equilibrium states (54). Reaching each of those states would require the system to undergo a partial liquid-to-solid phase transition, i.e., in our case, a protein aggregation. Upon an increase in temperature, the system tends to overcome an energy-activation barrier (nucleation) and reach a lower energy-equilibrium state via a type I aggregation transition. However, this new state in itself is a metastable one and, in turn, at certain destabilizing conditions such as higher temperatures, could become a transient route toward reaching an even lower energy-*stable* equilibrium state, via type II transition. The necessity for a sequential type I $\rightarrow$ type II mechanism is driven by the favorable (for type II) activation energy barrier provided by type I aggregate formation and its subsequent rearrangement (pseudonucleation). In this case, the entire type I aggregation process could be viewed in itself as a nucleation step for the type II aggregation of human IL-1ra at elevated temperatures.

Taken together, our experimental data support the sequential type I $\rightarrow$ type II mechanism. Still, the possibility of other mechanisms should not be dismissed. For example, an alternative ''parallel'' model implies a kinetic, structural, and thermodynamic uncoupling of the type II aggregation event, presumably via a separate type I-independent nucleation step. Future studies are needed to verify these hypotheses.

Our thanks go to Stephen Kaufman, Christine Siska, and Peter Quan for technical support, and Scott Silbiger for careful reading of the manuscript. We are also grateful to Tiansheng Li, Aichun Dong, Bruce Kerwin, Alex Shoshitaishvili, and David Brems for fruitful discussions.

REFERENCES

1. Cleland, J. F., M. F. Powell, and S. J. Shire. 1993. The development of stable protein formulations: a close look at protein aggregation, deamidation, and oxidation. *Crit. Rev. Ther. Drug Carrier Syst.* 10:307–377.
2. Carpenter, J. F., B. S. Kendrick, B. S. Chang, M. C. Manning, and T. W. Randolph. 1999. Inhibition of stress-induced aggregation of protein therapeutics. *Methods Enzymol.* 309:236–255.
3. Fink, A. L. 1998. Protein aggregation: folding aggregates, inclusion bodies and amyloid. *Fold. Des.* 3:R9–R23.
4. Manning, M. C., K. Patel, and R. T. Borchardt. 1989. Stability of protein pharmaceuticals. *Pharm. Res.* 6:903–918.
5. Koo, E. H., P. T. Lansbury, and J. W. Kelly. 1999. Amyloid diseases: abnormal protein aggregation in neurodegeneration. *Proc. Natl. Acad. Sci. USA.* 96:9989–9990.
6. Hardy, J., and D. J. Selkoe. 2002. The amyloid hypothesis of Alzheimer's disease: progress and problems on the road to therapeutics. *Science.* 297:353–356.
7. Kyle, R. A. 1994. Monoclonal proteins and renal disease. *Annu. Rev. Med.* 45:71–77.
8. Kendrick, B. S., B. S. Chang, T. Arakawa, B. Peterson, T. W. Randolph, et al. 1997. Preferential exclusion of sucrose from recombinant interleukin-1 receptor antagonist: role in restricted conformational mobility and compaction of native state. *Proc. Natl. Acad. Sci. USA.* 94:11917–11922.
9. Smith, A. V., and C. K. Hall. 2001. Protein refolding versus aggregation: computer simulation on an intermediate-resolution protein model. *J. Mol. Biol.* 312:187–202.
10. Chi, E. Y., S. Krishnan, T. W. Randolph, and J. F. Carpenter. 2003. Physical stability of proteins in aqueous solution: mechanism and driving forces in nonnative protein aggregation. *Pharm. Res.* 20:1325–1336.
11. Krishnan, S., E. Y. Chi, J. N. Webb, et al. 2002. Aggregation of granulocyte colony stimulating factor under physiological conditions: characterization and thermodynamic inhibition. *Biochemistry.* 41: 6422–6431.
12. Webb, J. N., S. D. Webb, J. L. Cleland, J. F. Carpenter, and T. W. Randolph. 2001. Partial molar volume, surface area, and hydration changes for equilibrium unfolding and formation of aggregation transition state:

high-pressure and co-solute studies on recombinant human IFN-gamma. *Proc. Natl. Acad. Sci. USA.* 98:7259–7264.

13. Wood, S. J., J. Wypych, S. Steavenson, J. C. Louis, M. Citron, et al. 1999. α-synuclein fibrillogenesis is nucleation-dependent. Implications for the pathogenesis of Parkinson's disease. *J. Biol. Chem.* 274:19509–19512.
14. Ferrone, F. 1999. Analysis of protein aggregation kinetics. *Methods Enzymol.* 309:256–274.
15. Kim, Y. S., S. P. Cape, E. Chi, R. Raffen, P. Wilkins-Stevens, et al. 2001. Counteracting effects of renal solutes on amyloid fibril formation by immunoglobulin light chains. *J. Biol. Chem.* 276:1626–1633.
16. Thirumalai, D., D. K. Klimov, and R. I. Dima. 2003. Emerging ideas on the molecular basis of protein and peptide aggregation. *Curr. Opin. Struct. Biol.* 13:146–159.
17. Fandrich, M., M. A. Fletcher, and C. M. Dobson. 2001. Amyloid fibrils from muscle myoglobin. *Nature.* 410:165–166.
18. Vetri, V., C. Canale, A. Relini, F. Librizzi, V. Militello, et al. 2007. Amyloid fibrils formation and amorphous aggregation in concanavalin A. *Biophys. Chem.* 125:184–190.
19. Nielsen, L., S. Frokjaer, J. Brange, V. N. Uversky, and A. L. Fink. 2001. Probing the mechanism of insulin fibril formation with insulin mutants. *Biochemistry.* 40:8397–8409.
20. Sambashivan, S., Y. Liu, M. R. Sawaya, M. Gingery, and D. Eisenberg. 2005. Amyloid-like fibrils of ribonuclease A with three-dimensional domain-swapped and native-like structure. *Nature.* 437:266–269.
21. Hills, R. D. Jr., and C. L. Brooks III. 2007. Hydrophobic cooperativity as a mechanism for amyloid nucleation. *J. Mol. Biol.* 368:894–901.
22. Raman, B., E. Chatani, M. Kihara, T. Ban, M. Sakai, et al. 2005. Critical balance of electrostatic and hydrophobic interactions is required for β2-microglobulin amyloid fibril growth and stability. *Biochemistry.* 44:1288–1299.
23. Ruano, M. L. F., I. Garcia-Verdugo, E. Miguel, J. Perez-Gil, and C. Casals. 2000. Self-aggregation of surfactant protein A. *Biochemistry.* 39:6529–6537.
24. Wang, K., and B. I. Kurganov. 2003. Kinetics of heat- and acidification-induced aggregation of firefly luciferase. *Biophys. Chem.* 106:97–109.
25. Raibekas, A. A., E. J. Bures, C. C. Siska, T. Kohno, R. F. Latypov, et al. 2005. Anion binding and controlled aggregation of human interleukin-1 receptor antagonist. *Biochemistry.* 44:9871–9879.
26. Roberts, C. J. 2007. Non-native protein aggregation kinetics. *Biotechnol. Bioeng.* 98:927–938.
27. Frieden, C. 2007. Protein aggregation processes: in search of the mechanism. *Protein Sci.* 16:2334–2344.
28. Liu, J., J. D. Andya, and S. J. Shire. 2006. A critical review of analytical ultracentrifugation and field flow fractionation methods for measuring protein aggregation. *AAPS J.* 8:E580–E589.
29. Latypov, R. F., T. S. Harvey, D. Liu, P. V. Bondarenko, T. Kohno, et al. 2007. Biophysical characterization of structural properties and folding of interleukin-1 receptor antagonist. *J. Mol. Biol.* 368:1187–1201.
30. Arend, W. P. 2002. The balance between IL-1 and IL-1ra in disease. *Cytokine Growth Factor Rev.* 13:323–340.
31. Murzin, A. G., A. M. Lesk, and C. Chothia. 1992. β-trefoil fold. Patterns of structure and sequence in the Kunitz inhibitors interleukins-1 β and 1 α and fibroblast growth factors. *J. Mol. Biol.* 223:531–543.
32. Vigers, G. P. A., P. Caffes, R. J. Evans, R. C. Thompson, S. P. Eisenberg, et al. 1994. X-ray structure of interleukin-1 receptor antagonist at 2.0-Å resolution. *J. Biol. Chem.* 269:12874–12879.
33. Schreuder, H. A., J. M. Rondeau, C. Tardif, A. Soffientini, E. Sarubbi, et al. 1995. Refined crystal structure of the interleukin-1 receptor antagonist. Presence of a disulfide link and a cis-proline. *Eur. J. Biochem.* 227:838–847.
34. Ansevin, A. T., and M. A. Lauffer. 1963. Polymerization-depolymerization of tobacco mosaic virus protein. I. Kinetics. *Biophys. J.* 3:239–251.
35. Smith, C. E., and M. A. Lauffer. 1967. Polymerization-depolymerization of tobacco mosaic virus protein. VIII. Light-scattering studies. *Biochemistry.* 6:2457–2465.
36. Jarrett, J. T., and P. T. Lansbury, Jr. 1992. Amyloid fibril formation requires a chemically discriminating nucleation event: studies of an amyloidogenic sequence from the bacterial protein OsmB. *Biochemistry.* 31:12345–12352.
37. Dong, A., and W. S. Caughey. 1994. Infrared methods for study of hemoglobin reactions and structures. *Methods Enzymol.* 232:139–175.
38. Kendrick, B. S., A. Dong, S. D. Allison, M. C. Manning, and J. F. Carpenter. 1996. Quantitation of the area of overlap between second-derivative amide I infrared spectra to determine the structural similarity of a protein in different states. *J. Pharm. Sci.* 85:155–158.
39. Seefeldt, M. B., Y. S. Kim, K. P. Tolley, J. Seely, J. F. Carpenter, et al. 2005. High pressure studies of aggregation of recombinant human interleukin-1 receptor antagonist: thermodynamics, kinetics and application of accelerated formulation studies. *Protein Sci.* 14:2258–2266.
40. Fogler, H. S. 2006. Collection and analysis of rate data. *In* Elements of Chemical Reaction Engineering, 4th ed. Prentice Hall, Upper Saddle River, NJ. 277–279.
41. Roy, S., D. Katayama, A. Dong, B. A. Kerwin, T. W. Randolph, et al. 2006. Temperature dependence of benzyl alcohol and 8-anilinonaphthalene-1-sulfonate-induced aggregation of recombinant human interleukin-1 receptor antagonist. *Biochemistry.* 45:3898–3911.
42. Latypov, R. F., D. Liu, K. Gunasekaran, T. S. Harvey, V. I. Razinkov, et al. 2008. Structural and thermodynamic effects of ANS binding to human interleukin-1 receptor antagonist. *Protein Sci.* 17:652–663.
43. Sehorn, M. G., S. V. Slepenkov, and S. N. Witt. 2002. Characterization of two partially unfolded intermediates of the molecular chaperone DnaK at low pH. *Biochemistry.* 41:8499–8507.
44. Hoyer, W., T. Antony, D. Cherny, G. Heim, T. M. Jovin, et al. 2002. Dependence of α-synuclein aggregate morphology on solution conditions. *J. Mol. Biol.* 322:383–393.
45. Kim, Y. S., T. W. Randolph, F. J. Stevens, and J. F. Carpenter. 2002. Kinetics and energetics of assembly, nucleation, and growth of aggregates and fibrils for an amyloidogenic protein. Insights into transition states from pressure, temperature, and co-solute studies. *J. Biol. Chem.* 277:27240–27246.
46. Giasson, B. I., K. Uryu, J. Q. Trojanowski, and V. M.-Y. Lee. 1999. Mutant and wild type human α-synucleins assemble into elongated filaments with distinct morphologies in vitro. *J. Biol. Chem.* 274:7619–7622.
47. Narhi, L., S. J. Wood, S. Steavenson, Y. Jiang, G. M. Wu, et al. 1999. Both familial Parkinson's disease mutations accelerate α-synuclein aggregation. *J. Biol. Chem.* 274:9843–9846.
48. Guo, B., S. Kao, H. McDonald, A. Asanov, L. L. Combs, et al. 1999. Correlation of second viral coefficients and solubilities useful in protein crystal growth. *J. Cryst. Growth.* 196:424–433.
49. Haas, C., and J. Drenth. 1999. Understanding protein crystallization on the basis of the phase diagram. *J. Cryst. Growth.* 196:388–394.
50. Cerda-Costa, N., A. Esteras-Chopo, F. X. Aviles, L. Serrano, and V. Villegas. 2007. Early kinetics of amyloid fibril formation reveals conformational reorganisation of initial aggregates. *J. Mol. Biol.* 366:1351–1363.
51. Serio, T. R., A. G. Cashikar, A. S. Kowal, G. J. Sawicki, J. J. Moslehi, et al. 2000. Nucleated conformational conversion and the replication of conformational information by a prion determinant. *Science.* 289:1317–1321.
52. Chiti, F., N. Taddei, F. Baroni, C. Capanni, M. Stefani, et al. 2002. Kinetic partitioning of protein folding and aggregation. *Nat. Struct. Biol.* 9:137–143.
53. Meyer, P. S., J. W. Yung, and J. H. Ausubel. 1999. A primer on logistic growth and substitution: the mathematics of the Loglet lab software. *Technol. Forecast. Soc. Change.* 61:247–271.
54. Anderson, G. M. 2005. Defining our terms. *In* Thermodynamics of Natural Systems, 2nd ed. Cambridge University Press, New York. 10–30.